ELSEVIER

Journal of Alloys and Compounds 303–304 (2000) 364–370

Journal of ALLOYS AND COMPOUNDS

www.elsevier.com/locate/jallcom

Emission quantum yield of europium (III) mixed complexes with thenoyltrifluoroacetonate and some aromatic ligands

F.R.G. e Silva[a], J.F.S. Menezes[b], G.B. Rocha[a], S. Alves[a], H.F. Brito[b], R.L. Longo[a], O.L. Malta[a,*]

[a]*Departamento de Química Fundamental da UFPE-CCEN, Cidade Universitéria, Recife, PE 50670-901, Brazil*
[b]*Departamento de Química Fundamental, Instituto de Química da Universidade de Sao Paulo, 05508-900, Sao Paulo, SP, Brazil*

Abstract

We report the experimental determination and theoretical calculation of the 4f–4f emission quantum yield (q) and $^5D_0$ excited state lifetime in the Eu $(TTA)_3.n$L compounds (where TTA=thenoyltrifluoroacetonate, L denotes 1,10-phenantroline orp-tolyl sulfoxide and n=1 or 2). The experimental q values for these compounds vary significantly by changing the L ligand. The relation between the emission quantum yield and photophysical characteristics of the compounds is discussed. The calculations are carried out by using theoretical models for ligand–rare earth ion energy transfer processes and numerical solutions of the rate equations. Pathways for the intramolecular energy transfer process between the ligands and the rare earth ion are proposed. The theoretical results agree well with the experimental data for the compounds analyzed.

Keywords: Rare earth complexes; Emission quantum yield; Energy transfer

1. Introduction

When irradiated with ultraviolet light absorbed by the ligands, several rare earth β-diketone compounds show strong luminescence in their electronic spectra [1,2]. The 4f–4f intraconfigurational transitions exhibit narrow line emissions. This is a direct consequence of the fact that the 4f orbitals are well shielded from the chemical environment by the closed 5s and 5p external sub-shells. These properties enable them to be extremely sensitive as luminescent probes that can give information on small perturbations surrounding the rare earth ion.

The 4f–4f luminescence intensity depends on a balance between radiative and non-radiative processes in the compound. This is in general obtained from a set of appropriate rate equations involving the transition rates and the populations of the energy levels of both ligand and rare earth ion. A theoretical approach to intramolecular energy transfer processes in coordination compounds with rare earth ions has been recently developed [3]. In this model, both the direct and the exchange Coulomb interactions are taken into account [4], yielding analytical expressions for the transfer rates as well as the selection rules for these systems.

In previous papers we have studied some spectroscopic properties of the complexes $Eu(TTA)_3 2L$, where L= dibenzyl sulfoxide (DBSO) and H_2O, giving emphasis to the theoretical calculations of ligand–Eu^{3+} ion energy transfer rates and emission quantum yields [2,5]. In the present work we present the experimental determination and a theoretical calculation of the 4f–4f emission quantum yield and of the $^5D_0$ excited state lifetime for the $Eu(TTA)_3$PHEN and $Eu(TTA)_3 2$PTSO compounds, where PHEN=1,10-phenantroline and PTSO=*p*-tolyl sulfoxide. These compounds are highly luminescent. Our interest here is to analyze the influence of the ligand L on the luminescence of the Eu^{3+} ion and to elucidate which parameters govern its emission yield. The good agreement found between theoretical and experimental q values provides a further support to the theoretical scheme that has been proposed in the study and modeling of efficient light converting molecular devices [2].

2. Experimental detail

2.1. Synthesis and characterization

The compound $RE(TTA)_3$PHEN (RE=Eu^{3+} and Gd^{3+}) was prepared by the method described by Melby et al. [6]. The solid product was recrystallized from 95% alcohol and

*Corresponding author. Tel.: 55-81-2718-441; fax: 55-8-2718-442.
E-mail address: omlm@npd.ufpe.br (O.L. Malta)

0925-8388/00/$ – see front matter
PII: S0925-8388(00)00642-3

dried under vacuum over anhydrous calcium chloride in a desiccator at room temperature overnight.

The europium content was determined by complexometric titration with EDTA in methanol [7]. The carbon, hydrogen and nitrogen contents were estimated by microanalytical procedures. The C, H, N and RE percentage values found/calculated for the complexes are: $Eu(TTA)_3PHEN$ (C, 43.38/43.42; H, 2.21/2.02; N, 2.70/2.81; Eu^{3+}, 15.18/15.26) and $Gd(TTA)_3PHEN$ (C, 43.0/43.20; H, 1.96/2.0; N, 2.85/2.80; Gd^{3+}, 15.58/15.71). These percentage values for the complexes with the H_2O, DBSO and PTSO ligands are reported in Refs. [2,8].

The infrared spectra were measured at room temperature in a Perkin-Elmer 1750-FTIR spectrophotometer in the 4000–400 cm^{-1} spectral range. The KBr plates and nujol mull suspension techniques for the compound and films of the free ligand were applied. The ER spectra show the displacement of the C–N stretching from 1643 cm^{-1} in the free PHEN ligand to 1622 cm^{-1} in the compounds and the displacement of the C=O stretching from 1680 cm^{-1} in the free TTA ligand to 1600 cm^{-1} in the compounds provides good evidence that the metal ion is coordinated through the oxygen and nitrogen atoms [2,9].

2.2. Absorption and luminescence spectra

The absorption spectra of the $Eu(TTA)_3PHEN$ and $Eu(TTA)_32PTSO$ compounds dissolved in ethanol were measured in a UV-visible spectrophotometer LAMBDA 6 model 2688-002. Four bands peaked at 342 nm, 264 nm, 230 nm and 201 nm are observed in $Eu(TTA)_3PHEN$ and four bands peaked at 339 nm, 265 nm, 240 nm and 202 nm are also observed in $Eu(TTA)_32PTSO$. The absorption spectra of the remaining compounds are very similar. These bands correspond to singlet-to-singlet transitions in the ligands, and due to the similarities between the spectra we may conclude that they are mainly localized in the TTA ligands.

The luminescence spectra of the $Eu(TTA)_32DBSO$, $Eu(TTA)_32H_2O$ and $Eu(TTA)_32PTSO$ compounds have been presented in Refs. [2] and [8]. The luminescence spectrum of the $Eu(TTA)_3PHEN$ sample was excited by a 150 W xenon lamp. The wavelengths were selected by a 0.25 monochromator (Jobin Yvon Model H-10). The emission spectra were analyzed by a Jobin Yvon double monochromator (model U-1000) and the signal, detected by a water-cooled RCA C3 1034-02 photomultiplier, was processed by a Jobin Yvon Spectralink system. The luminescence spectra of the $Gd(TTA)_32PTSO$ and $Gd(TTA)_3PHEN$ samples at 77 K were excited by a nitrogen laser model VSL-337 ND. They are shown in Figs. 1 and 2, in the spectral region from 400 to 700 nm. The emission band centered around 550 nm for $Gd(TTA)_3PHEN$ and around 527 nm for $Gd(TTA)_32PTSO$ is actually composed of three phosphorescence bands corresponding to the emission from the lowest three triplet

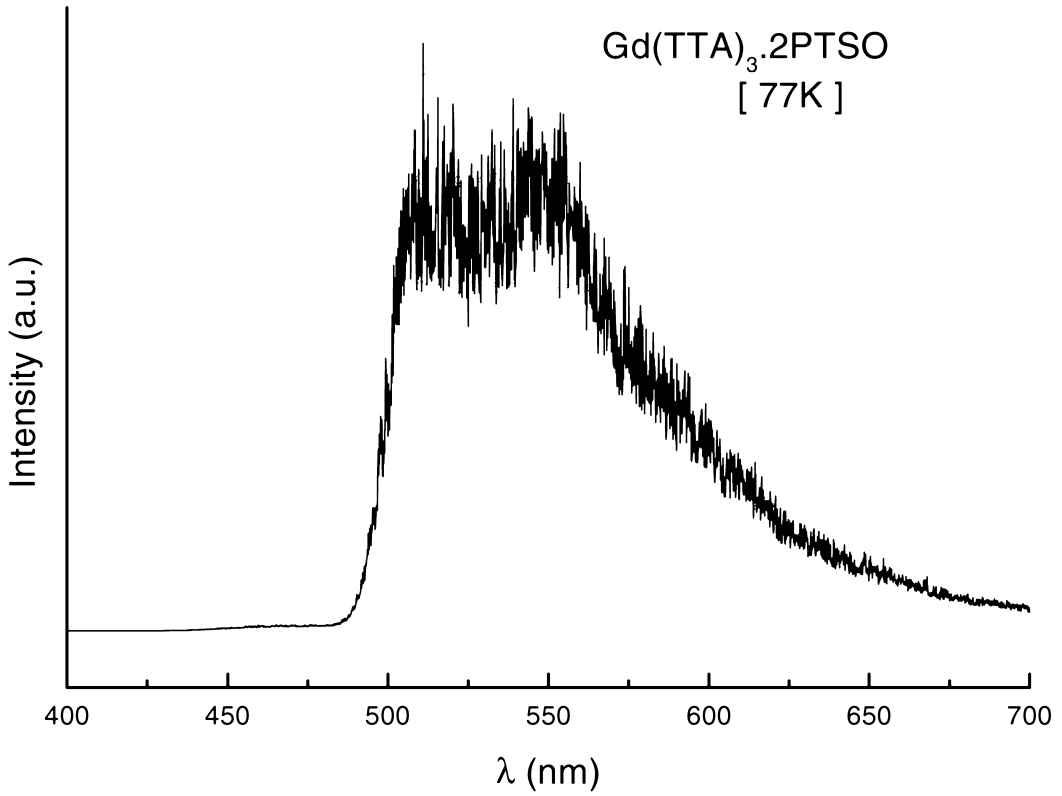

Fig. 1. Emission spectrum of the compound $Gd(TTA)_32PTSO$, at 77 K, under excitation at 337 nm (nitrogen laser).

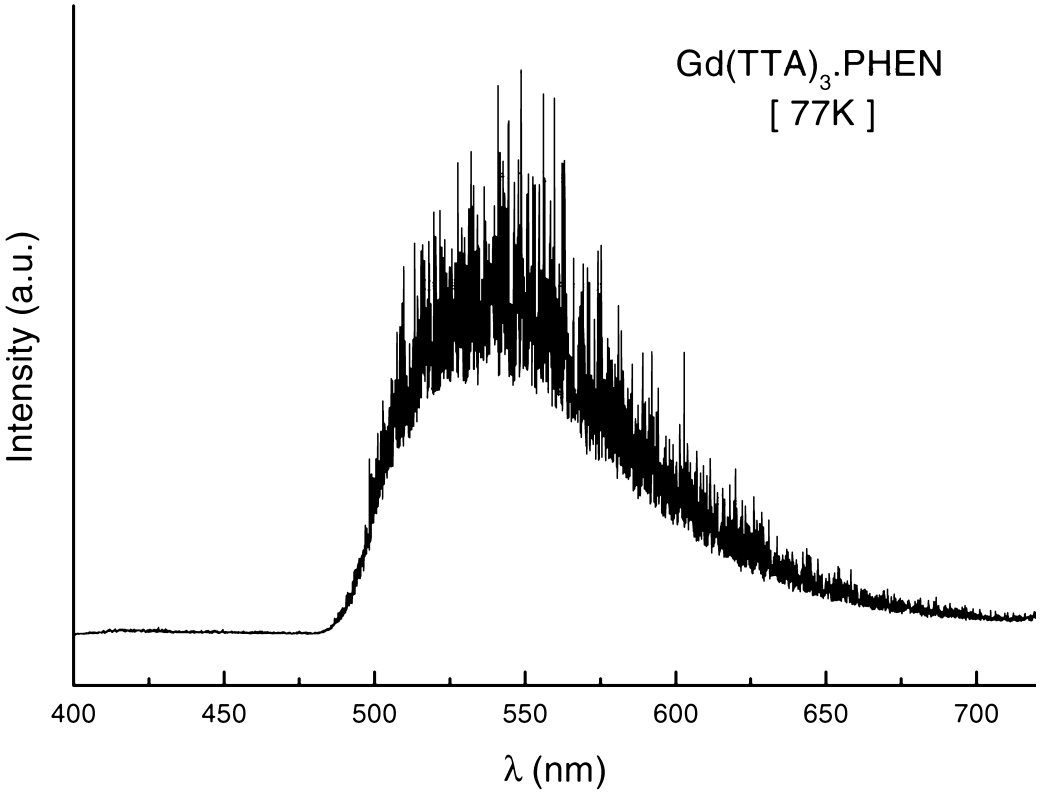

Fig. 2. The same as in Fig. 1 for the $Gd(TTA)_3PHEN$ compound.

states, each localized in a TTA ligand molecule, as shown by our lifetime measurements and electronic structure calculations presented in the following sections.

2.3. Quantum yield and lifetime measurements

The emission quantum yield q for the $Eu(TTA)_3 2PTSO$ and $Eu(TTA)_3PHEN$ compounds were obtained following the procedure described in Ref. [5]. The q value is defined as the ratio between the number of photons emitted by the Eu^{3+} ion and the number of photons absorbed by the ligands. According to the method developed by Bril and coworkers at Philips Research Laboratories [10], the q value for a given sample can be determined by comparison with standard phosphors, whose quantum yields have been previously determined by absolute measurements. This method provides absolute yields while avoiding absolute measurements, which are in general complicated. The quantum yield q_x of a sample is thus determined as follows

$$q_x = \left(\frac{1 - r_{ST}}{1 - r_x}\right)\left(\frac{\Delta\Phi_x}{\Delta\Phi_{ST}}\right) q_{ST}$$

where r_{ST} and r_x are the amount of exciting radiation reflected by the standard and by the sample, respectively, and q_{ST} is the quantum yield of the standard phosphor. The terms $\Delta\Phi_x$ and $\Delta\Phi_{ST}$ give the integrated photon flux (photons s^{-1}) for the sample and the standard phosphor, respectively.

The standard in our case was sodium salicylate (Merck P.A.), which has a broad emission band with a maximum at 450 nm and $q = 60\%$ at room temperature [11]. The results show that the method is accurate within 10%, in agreement with the accuracy reported in Ref. [10].

The lifetime measurements were made for the $RE(TTA)_3 2PTSO$ and $RE(TTA)_3PHEN$ compounds, where $RE = Eu^{3+}$ and Gd^{3+}, at 298 and 77 K, using the nitrogen laser for excitation purposes and a Box Car system (EG&G Princeton Applied Research) for data acquisition. The results are presented in Table 1. The

Table 1
Lifetimes of the emitting levels in the $RE(TTA)_3 2PTSO$ and $RE(TTA)_3PHEN$ compounds. The values for the Eu^{3+} compounds are at room temperature and those for the Gd^{3+} compounds are at 77 K

Compound	$Eu(TTA)_3 2PTSO$	$Gd(TTA)_3 2PTSO$	$Eu(TTA)_3PHEN$	$Gd(TTA)_3PHEN$
Lifetimes (ms)	0.598	2.032	0.976	3.465

luminescence lifetimes for the Gd^{3+} compounds are considerably high. This is consistent with emission from a state with a strong triplet character.

3. Theory

3.1. Ligand–rare earth ion energy transfer rate

According to the theoretical model developed recently [3,4], the following expressions have been obtained for the ligand–rare earth ion energy transfer rate W_{ET}

$$W_{ET} = \frac{2\pi}{\hbar}\frac{e^2 S_L}{(2J+1)G} F \sum_{\lambda} \gamma_\lambda \langle \alpha' J' \| \mathbf{U}^{(\lambda)} \| \alpha J \rangle^2 \quad (1)$$

which corresponds to the dipole–2^λ pole mechanism ($\lambda =$ 2, 4 and 6),

$$W_{ET} = \frac{2\pi}{\hbar}\frac{e^2 S_L}{(2J+1)GR_L^6} F \sum_{\lambda} \Omega_\lambda^{e.d.} \langle \alpha' J' \| \mathbf{U}^{(\lambda)} \| \alpha J \rangle^2 \quad (2)$$

corresponding to the dipole–dipole mechanism ($\lambda = 2,4$ and 6), and

$$W_{ET} = \frac{8\pi}{3\hbar}\frac{e^2(1-\sigma_0)^2}{(2J+1)R_L^4} F \langle \alpha' J' \| S \| \alpha J \rangle^2 \sum_m |\langle \phi | \sum_k \mu_z(k) s_m(k) | \phi' \rangle|^2 \quad (3)$$

corresponding to the exchange mechanism. In the above equations J represents the total angular momentum quantum number of the rare earth ion and a specifies a 4f spectroscopic term. G is the degeneracy of the ligand initial state and S_L is the electric dipole strength associated with the transition $\phi \rightarrow \phi'$ in the ligand. The quantities $\langle \| \ \| \rangle$ are reduced matrix elements of the unit tensor operators $\mathbf{U}^{(\lambda)}$ [12], and R_L is the distance from the rare earth ion nucleus to the region of the ligand molecule in which the ligand donor (or acceptor) state is localized [3]. In Eq. (3) S is the total spin operator of the rare earth ion, μ_z is the z component of the electric dipole operator and $s_m (m = 0, \pm 1)$ is a spherical component of the spin operator, both for the ligand electrons, and σ_0 is a distance dependent screening factor [2].

The matrix elements $\langle \phi | \Sigma_k \ \mu_z(k) s_m(k) | \phi' \rangle$ were calculated from the molecular orbital wave functions given by the sparkle model as described in Ref. [2]. This model, which has been recently introduced and described in Refs. [13,14], leads to optimized coordination geometries, and electronic structure of the organic part of rare earth coordination compounds.

The quantities γ_λ and F are given by

$$\gamma_\lambda = (\lambda + 1)\frac{\langle r^\lambda \rangle^2}{(R_L^{\lambda+2})^2} \langle 3 \| \mathbf{C}^{(\lambda)} \| 3 \rangle^2 (1 - \sigma_\lambda)^2 \quad (4)$$

and

$$F = \frac{1}{\hbar\gamma_L}\sqrt{\frac{\ln 2}{\pi}} \exp\left[-\left(\frac{\Delta}{\hbar\gamma_L}\right)^2 \ln 2 \right] \quad (5)$$

where $\langle r^\lambda \rangle$ is the radial expectation value of r^λ for 4f electrons, $\mathbf{C}^{(\lambda)}$ is a Racah tensor operator [15] and the σ_λ's are also screening factors [16,17]. γ_L is the ligand state bandwidth at half-height and Δ is the difference between the donor and acceptor transition energies involved in the transfer process.

The selection rules that can be derived from the above equations are the following: $J + J' \geq \lambda \geq |J - J'|$, for the mechanisms expressed by Eqs. (1) and (2), and $\Delta J = 0$, ± 1, for the exchange mechanism, Eq. (3), in both cases $J' = J = 0$ excluded. From the ligand side the selection rules can be derived from the electric dipole strength S_L and the matrix element of the coupled operators μ_z and s_m in Eq. (3). The theoretical procedures for using the above equations and the corresponding selection rules have been discussed in detail in the previous publications [2,18].

3.2. Rate equations

The normalized level populations, η_i, are described by a set of rate equations which have the general form

$$\frac{d\eta_i}{dt} = -\sum_{\substack{j=1 \\ j\neq i}}^{N} k_{ij}\eta_i + \sum_{\substack{j=1 \\ j\neq i}}^{N} k_{ji}\eta_j \quad (6)$$

where the indices i and j indicate the energy levels in the compound involved in the energy transfer process. k_{ij} or k_{ji} correspond to the transition and transfer rates between the i and j levels, or j and i levels, respectively, and N is the total number of levels involved. In the steady state regime all the $d\eta_i/dt$ are equal to zero, and the set of algebraic equations can be solved analytically in terms of the transition and transfer rates [5].

In the present case the rate equations were solved numerically by using the 4-th order Runge–Kutta method with an adaptive integration step [19]. This set of coupled differential equations belongs to the initial value category, where the populations (η_i) at $t = 0$ were set equal to 1, for the ground state population, and to zero for the other states. The total time of propagation was around 0.01 s and the initial step size was equal to the inverse of the largest transfer rate (approximately 10^{-9} s).

The numerical solutions of the rate equations yield the time dependence of the energy level populations, which reach the steady-state regime after $10^{-6}-10^{-5}$ s. These steady-state populations were then used to calculate the emission quantum yield which is given by

$$q = \frac{A_T \eta_2}{\phi \eta_1} \quad (7)$$

where the sub-indices 1 and 2 indicate the ground state and

the emitting level ($^5D_0$), respectively, in the complex, A_T is the sum of the coefficients of spontaneous emission for the $^5D_0 \rightarrow {}^7F_{0,1,2,4}$ transitions and ϕ is the pumping rate.

3.3. Lifetimes

The procedure for the calculation of excited state lifetimes has been described in Ref. [19]. After the populations have reached a steady-state behaviour the pumping rate (ϕ) is set equal to zero, the rate equations are propagated, and the time dependence of the populations are obtained. We assume that the lifetime is then obtained simply by determining the time at which the population of the state of interest decays an amount of $1/e$, in the same way as it was determined experimentally from the corresponding luminescence decay curve.

4. Results and discussion

An energy level diagram for the compounds $Eu(TTA)_3$2PTSO and $Eu(TTA)_3$PHEN is shown in Fig. 3. It is similar to the diagram considered for the compounds $Eu(TTA)_3$2DBSO and $Eu(TTA)_3 2H_2O$ [5]. The UV absorption takes place through the TTA ligands, for which the lowest triplet and singlet states were determined experimentally from the absorption, excitation and phosphorescence spectra of the compounds $RE(TTA)_3$2PTSO and $RE(TTA)_3$PHEN. There are three 4f levels in $Eu(TTA)_3$2PTSO and $Eu(TTA)_3$PHEN that show appropriate resonance conditions with the TTA excited energy levels. This figures also labels the energy levels involved in the mechanism as well as transfer and transition rates involved (k_{ij}). The choice of the $^5D_0$,$^5D_1$ and $^5D_4$ states of the Eu^{3+} ion for the energy transfer process was due to the resonance conditions and the selection rules derived in Refs. [3,4] (Section 3).

The lowest singlet and triplet theoretical energies are 30 800 cm^{-1} and 20 525 cm^{-1} for $Eu(TTA)_3$2PTSO, and 30 097 cm^{-1} and 19 814 cm^{-1} for $Eu(TTA)_3$PHEN, respectively. These theoretical energies were calculated from the sparkle model. In the case of the triplet states an average value for the three TTA ligands is given. These results are in satisfactory agreement with the experimental values.

Table 2 presents the theoretical values of the forward and back-transfer rates calculated from Eqs. (1)–(3). The arrows in this table indicate the direction of the energy

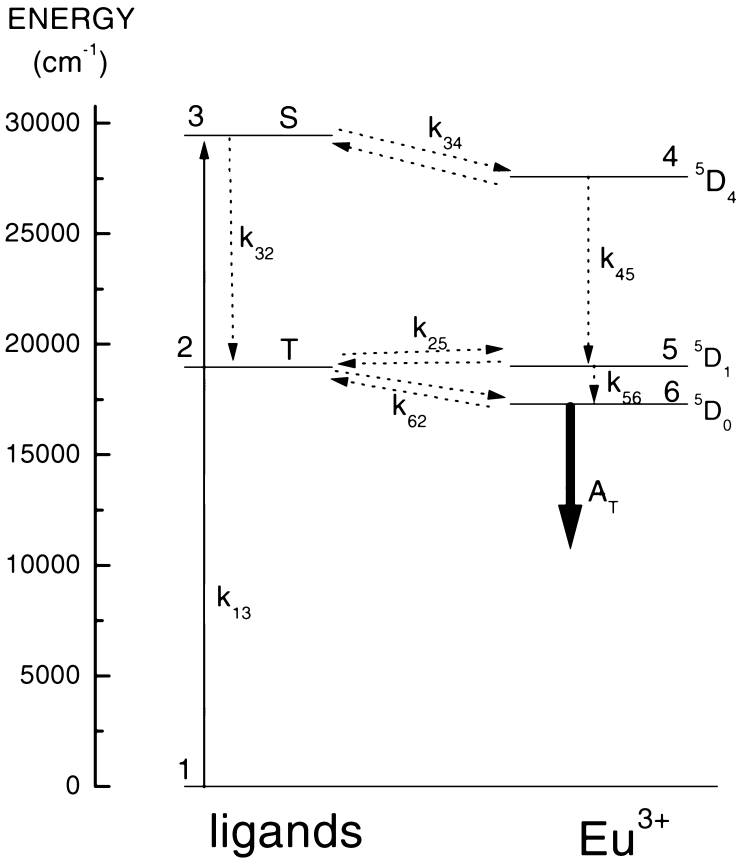

Fig. 3. Energy level diagram for the $Eu(TTA)_3$2PTSO and $Eu(TTA)_3$PHEN compounds showing the most probable channels for the intramolecular energy transfer process. The full lines represent radiative processes; the dotted lines represent non-radiative processes. The pumping rate is k_{13}. k_{32} and A_T are the intersystem crossing rates and the total Einstein's coefficient of spontaneous emission, respectively.

Table 2
Calculated values for the energy transfer rates $Eu(TTA)_3PHEN$ compounds

Ligand state (cm^{-1})	4f State (cm^{-1})	Transfer rate (s^{-1})	Back-transfer rate (s^{-1})
$Eu(TTA)_3$2PTSO			
Triplet (18 963)→$^5D_0$ (17 300)		k_{26}1.54×10^8	$k_{62}=1.34\times10^4$
Triplet (18 963)←$^5D_1$ (19 070)		k_{52}1.21×10^9	$k_{25}=7.27\times10^8$
Singlet (29 464)→$^5D_4$ (27 600)		$k_{34}=4.47\times10^{6a}$	$k_{43}=621$
$Eu(TTA)_3PHEN$			
Triplet (18 182)→$^5D_0$ (17 300)		$k_{26}=4.10\times10^8$	$k_{62}=1.47\times10^6$
Triplet (18 182)←$^5D_1$ (19 070)		$k_{52}=2.51\times10^9$	$k_{25}=3.65\times10^7$
Singlet (29 240)→$^5D_4$ (27 600)		k_{34} 5.13×10^{6a}	$k_{43}=1.55\times10^4$

[a] Dipole–dipole mechanism.

transfer and the energy level labeling is presented in Fig. 3. The forward transfer rate to the $^5D_0$ level was calculated by assuming a thermal population factor equal to 0.17, at 300 K, for the $^7F_1$ manifold and an energy difference $\Delta=E(\text{triplet})-[E(^5D_0)-E(^7F_1)]$. The parameters used in the calculations of the transfer rates were obtained from the luminescence spectra, lifetime measurements and sparkle model (structural data and ligand matrix elements). The parameters for $Eu(TTA)_3$2PTSO were $R_L=4.3$ Å (average value), $\gamma_{triplet}=3022$ cm^{-1}, $A_T=1119$ s^{-1} and the theoretical value used for the z-component of the electric dipole matrix element in Eq. (3) was 1.92×10^{-36} $(e.s.u.)^2$ cm^2. The inverse of the lifetime $(1/\tau)$ was set to 1672 s^{-1}. In addition, the multipolar contributions to the transfer rates were calculated by using the following theoretical values for $\Omega_\lambda^{e.d.}$ (in 10^{-20} cm^2): $\Omega_\lambda^{e.d.}=0.1$, $\Omega_\lambda^{e.d.}=0.22$ and $\Omega_6^{e.d.}=0.4$. In the case of $Eu(TTA)_3PHEN$ we used the following parameters: $R_L=4.5$ Å (average value), $\gamma_{triplet}=3198$ cm^{-1}, $A_T=669$ s^{-1} and 5.34×10^{-36} $(e.s.u.)^2$ cm^2 for the squared matrix element of the coupled spin–dipole operator in Eq. (3). The inverse of the lifetime $(1/\tau)$ was 1025 s^{-1}. The theoretical values for $\Omega_\lambda^{e.d.}$ (in 10^{-20} cm^2) were: $\Omega_2^{e.d.}=0.18$, $\Omega_2^{e.d.}=0.29$ and $\Omega_6^{e.d.}=0.55$. It should also be noticed that the back-transfer rates were calculated by multiplying the forward transfer rates by the Boltzmann factor $e^{-|\Delta|/k_BT}$ at room temperature. We also have assumed that the value of the non-radiative decay rate of the 4f–4f transitions within a $4f^N$ electronic configuration is 10^6 s^{-1}, which indeed corresponds to the decay from the $^5D_1$ to the $^5D_0$ level.The following values for the screening factors were assumed for these compounds, $\sigma_2=0.6$, $\sigma_4=0.139$, $\sigma_6=-0.1$ and $\sigma_0=0.989$ [2].

The energy transfer rates involving both singlet and triplet states are considerably high for the compounds presented in Table 2. They are higher for the $^5D_0$ and $^5D_1$ levels, where the exchange interaction dominates, than for the higher excited 4f levels, where the multipolar interactions are the most important ones. The multipolar interactions include the dipole–dipole and dipole–2^l–dipole mechanisms. However, only the dipole–dipole mechanism gives a significant contribution to the multipolar transfer rate.

The measured emission quantum yields for the Eu^{3+} ion, according to the procedure described in Section 2.3, were 57%, for the compound with PTSO, and 69%, for the compound with PHEN, at room temperature. These experimental q values together with those for the $Eu(TTA)_3$2DBSO and $Eu(TTA)_3$2H_2O compounds are presented in Table 3. The emission quantum yield corresponds to the $^5D_0\rightarrow{}^7F_{0,1,2,3,4}$ transitions. To compare theory with experiment, the numerical solution of the rate equations, Eq. (6), has been performed and the steady-state populations have been obtained for all the energy levels involved in the transfer process shown in Fig. 3. These populations were then employed in Eq. (7) to obtain the theoretical emission quantum yields. The calculations were performed by using the values of the energy transfer rates presented in Table 2 and also the following values of decay rates, $k_{21}=10^5$ s^{-1}, $k_{32}=10^8$ s^{-1}, $k_{31}=10^6$ s^{-1}, $k_{13}=10^4$ s^{-1} [19]. We find, from Eq. (7), an optimum emission quantum yield of 66% for the compound with PTSO. The corresponding value for the compound with PHEN is 63%, both in good agreement with experiment.

Table 3
Experimental and theoretical emission quantum yield, $^5D_0$ lifetime, and A_T values for the $Eu(TTA)_3$2PTSO, $Eu(TTA)_3PHEN$, $Eu(TTA)_3$2DBSO and $Eu(TTA)_3$2H_2O compounds

Compounds	A_T (s^{-1})	$1/\tau$ ($^5D_0$) Experimental (s^{-1})	$1/\tau$ ($^5D_0$) Theoretica1 (s^{-1})	($q_{EXP.}$) (%)	($q_{THEOR.}$) (%)
$Eu(TTA)_3$2DBSO	980	1400	–	85	70
$Eu(TTA)_3PHEN$	669	1025	1057	69	63
$Eu(TTA)_3$2PTSO	1119	1672	1675	57	66
$Eu(TTA)_3$2$H_2$0	1110	3840	–	23	29

These data and results are summarized in Table 3. For the sake of comparison the emission quantum yield, coefficient of spontaneous emission and experimental $^5D_0$ lifetime for the case of the $Eu(TTA)_3 2DBSO$ and $Eu(TTA)_3 2H_2O$ compounds, obtained in Refs. [2,5], are also shown.

We have observed in our calculations that the emission quantum yield is considerably affected by the k_{32} rate (S→T intersystem crossing) and by the k_{26}, k_{52} and k_{25} transfer rates, which are the highest rates indicated in Fig. 3. On the other hand, the k_{34} energy transfer rate (transfer via the ligand singlet state) weakly affects the process due to its low value ($\sim 10^6$ s^{-1}) compared to the k_{32} rate (10^8 s^{-1}). As a result, the most probable energy transfer channels in the compounds analyzed are: ground state $\rightarrow S \rightarrow T \rightarrow {}^5D_0$ emission and ground state $\rightarrow S \rightarrow T \rightarrow {}^5D_1 \rightarrow {}^5D_0 \rightarrow$ emission. The calculations also show that the q values, as expected, are modulated by the $^5D_0$ lifetime and by the spontaneous emission coefficient A_T. Among the non-hydrated compounds the $Eu(TTA)_3PHEN$ one has the lowest A_T, probably due to the fact that the PHEN ligand is more distant from the Eu^{3+} ion than the DBSO and PTSO ligands, contributing to a weaker ligand field interaction, and also by the fact that the PHEN nitrogen ligating atoms are less polarizable than the oxygens of DBSO and PTSO. On the other hand, this fact is balanced by the longer lifetime, in the case of the PHEN ligand, producing a high q value. Also, for this case, this indicates that multiphonon non-radiative deactivation of the $^5D_0$ level is less important than for the other compounds.

The numerical solution of the rate equations is quite efficient and much richer than the usual steady-state solution, since it can yield the time dependence of each population [19]. The time dependence of the $^5D_0$ population allowed us to calculate the lifetime of this level and to compare it with the experimental data. The results are presented in Table 3. The agreement between calculated and experimental results is noteworthy in the sense that it shows the consistency of our set of rate equations and corroborates the intramolecular pathways proposed in Fig. 3.

Effects of temperature on the emission quantum yields have not been studied due to experimental restrictions. Moreover, from the theoretical point of view the analysis of these effects would require a more precise definition of the temperature dependence of the energy transfer and non-radiative rates in our model. Actually, this is a subject which is under consideration in our project of description and modeling of these UV-visible light conversion compounds.

Acknowledgements

The authors acknowledge CAPES, CNPq, FINIP, FAPESP and PADCT (Brazilian agencies) for financial support. They are also grateful to Prof. C.M. Donegá for the helpful discussions.

References

[1] R.C. Holz, L.C. Thompson, Inorg. Chem. 27 (1988) 4641.
[2] O.L. Malta, H.F. Brito, J.F.S. Menezes, F.R. Gonçalves e Silva, S. Alves Jr., F.S. Farias Jr., A.M.V. de Andrade, J. Luminescence 75 (1997) 1.
[3] O.L. Malta, J. Luminescence 71 (1997) 229.
[4] F.R.G. Silva, O.L. Malta, J. Alloys Comp. 250 (1997) 427.
[5] O.L. Malta, H.F. Brito, J.F.S. Menezes, F.R. Gonçalves e Silva, C.S. Alves Jr., Chem. Phys. Lett. 282 (1998) 233.
[6] L.R. Melby, N.J. Rose, E. Abramson, J.C. Cans, J. Am. Chem. Soc. 86 (1964) 5117.
[7] S.J. Lyle, M.M. Rahman, Talanta 10 (1963) 1177.
[8] H.F. Brito, O.L. Malta, C.A.A. de Carvalho, J.F.S. Menezes, Ferraz, J. Alloys Comp., in press.
[9] G.F. de Sá, F.R.G. e Silva, O.L. Malta, J. Alloys Comp. 207/208 (1994) 457.
[10] A. Bril, W. De Jager-Veenis, J. Res. Nat. Bureau Stand. 80A (1976) 401.
[11] A. Bril, A.W. De Jager-Veenis, J. Electrochem. Soc. 123 (1976) 396.
[12] W.T. Carnall, H. Crosswhite, H.M. Crosswhite, Energy Structure and Transition Probabilities of the Trivalent Lanthanides in LaF_3, Argonne National Laboratory Report, unnumbered, 1997.
[13] A.V.M. de Andrade, N.B. da Costa Jr., A.M. Simas, G.F. de Sá, Chem. Phys. Lett. 227 (1994) 349.
[14] A.V.M. de Andrade, R.L. Longo, A.M. Simas, G.F. de Sá, J. Chem. Soc., Faraday Trans. 92 (1996) 1835.
[15] A.R. Edmonds, Angular Momentum in Quantum Mechanics, Princeton University Press, New Jersey, 1975.
[16] D.J. Newman, D.C. Price, J. Phys. C: Solid State Phys. 8 (1975) 2985.
[17] M. Faucher, D. Garcia, Phys. Rev. B26 (1982) 5451.
[18] O.L. Malta, F.R.G. e Silva, Spectrochim. Acta, Part A 54 (1998) 1593.
[19] O.L. Malta, F.R.G. e Silva, R. Longo, Chem. Phys. Lett. 307 (1999) 518.